Shimmy in Aircraft Landing Gear

Problem presented by

Etienne Coetzee

Airbus

Problem statement

Shimmy is an oscillation in the landing gear of an aircraft that can occur during taxiing, take-off or landing. Traditional shimmy analysis considers the effect to be linear. The Study Group considered a simplified nonlinear model for shimmy and studied its linear stability, and its nonlinear behaviour numerically, and showed that it has supercritical Hopf bifurcations. These results are broadly in agreement with observations of shimmy in some circumstances, but a more complex model would need to cover effects that are neglected here.

Study Group contributors

Maria Aguareles (Universitat Politècnica de Catalunya)
Sergei Anisov (Utrecht University)
Mahboubeh Asgari (UCL)
David Barton (University of Bristol)
Sunny Chiu-Webster (University of Cambridge)
Giles Hunt (University of Bath)
Joanna Mason (University of Bristol)
David Parker (University of Edinburgh)
David Rodrigues (University of Bristol)
Juan Sola-Morales (Universitat Politècnica de Catalunya)
Dominic Vella (University of Cambridge)
David Wood (University of Warwick)

Report prepared by

David Barton (University of Bristol)
David Wood (University of Warwick)

1   Introduction

Shimmy is an oscillation in aircraft landing gear that can occur both on landing and take-off, typically in a band of velocities. It causes excessive wear on components and can cause accidents. The nose wheel is roughly like a caster on a shopping trolley: the horizontal axle of the wheel is mounted in an assembly that is free to rotate about a vertical axis. Shimmy is (or at least includes) oscillation of the wheel assembly about this vertical axis. The current engineering approach has little understanding of the physical mechanisms causing shimmy, but relies on the use of shimmy dampers, and on systematic maintenance and replacement of landing gear components. Simulations are carried out with finite element models and multi-body systems, and there are theoretical models due to Stépán [3, 4] and Somieski [2]. In fact shimmy can also involve lateral oscillation of the landing gear (as well as torsional) and can be coupled to and caused by flutter of the airframe. The phenomenon is multi-scale in nature, as it can be linked to normal mechanical wear of key components at one scale, and gross flexibility effects at the vehicle scale. Airbus wish to identify it earlier in order to address passenger comfort, pilot comfort, manage mechanical wear and avoid over-fatiguing the system elements. Specifically, Airbus wish to identify key system elements that may cause shimmy, when given a particular configuration of an aircraft. At early stages of development the configuration may involve the shape and size of the fuselage and design of the landing gear, whilst at the other end of the development process, the configuration may also consist of detailed system elements such as actuators, *etc.* Airbus relies on systematic maintenance and replacement of landing gear components, thereby avoiding the occurrences of the abovementioned phenomena.

2   The model

The model we shall use here is largely taken from that of Somieski [2] and we shall use similar notation. A table of all our notation is given in Section 7.

2.1   Assumptions

The model only considers motion in the horizontal plane, and so essentially consists of

- a couple-acceleration model for rotation of the landing gear about the main vertical strut;

- a simple model for the dynamics of the tyre-ground interaction.

We discuss each of these in turn. The variables are introduced in Figure 1, where the x-axis is taken along the direction of the aircraft velocity, V. This is assumed prescribed and constant, so we are neglecting any effects due to the interaction of the landing gear with the aircraft. These are known to occur — in fact it has been observed that a landing
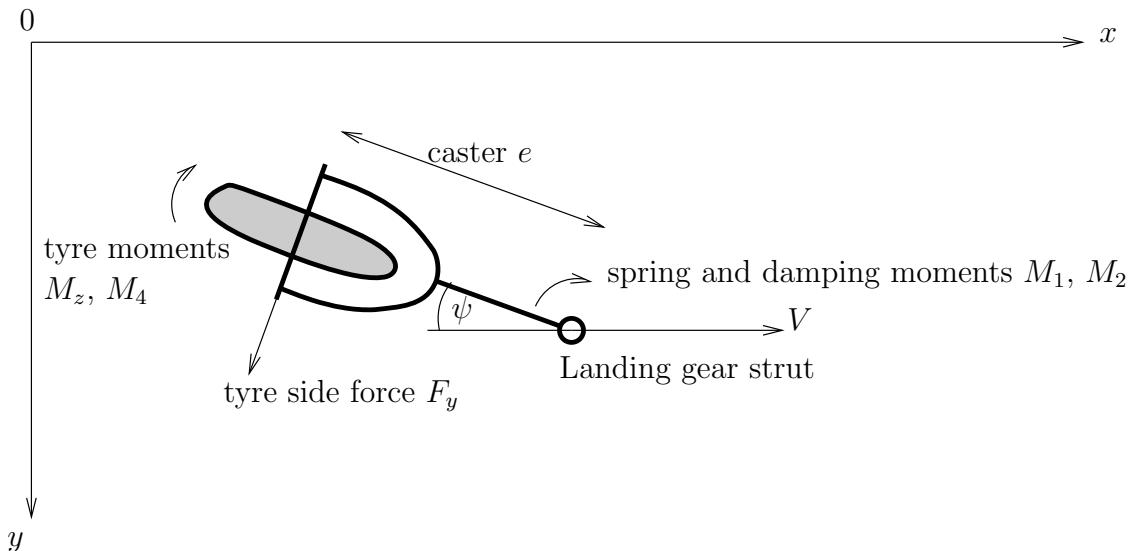
Figure 1: Schematic of landing gear (from Somieski [2]).

gear can be stable when run in isolation, but exhibits shimmy when it is run connected to the fuselage of a real aircraft: such effects are not included in this model, nor are lateral oscillations of the strut. Also, in thinking of V as constant, we are effectively looking for instabilities that occur on timescales short compared to the timescales over which V varies significantly. The instantaneous yaw angle of the landing gear about the strut is denoted by ψ, and its moment of inertia about the strut by I_z. The strut itself exerts moments on the landing gear which are denoted by

$$M_1(\psi) = c\psi, \qquad (c < 0); \qquad M_2(\dot{\psi}) = k\dot{\psi}, \qquad (k < 0). \tag{1}$$

So M_1 is the elastic torsional moment in the strut, and M_2 is a combined damping moment from the various damping mechanisms in the strut. These are considered linear in ψ and $\dot{\psi}$ respectively. The contact of the tyre with the ground is complex in reality: the tyre has some leading contact point with the ground, then a region of contact, and at the rear there will be some slip in the unloading region. Nevertheless, in this simplified model it is assumed that there is no slip, and that the position of the leading contact point defines the way the tyre contacts the ground. The deviation of the leading contact point from the x-axis is denoted by y_1 and this is assumed to follow the model

$$\dot{y}_1 + \frac{V}{\sigma}y_1 = V\psi + (e - a)\dot{\psi}. \tag{2}$$

Here σ is the relaxation length of transverse tyre deflections (*i.e.* deflections in the y-direction), e is the length of the caster arm as shown in Figure 1, and a is the half-length of the contact of the tyre with the ground. This is called an elastic string model, and further details are discussed by Stépán in [4] and in the references given by [2]. From y_1, an angle α, called the slip angle, is defined by

$$\alpha = y_1/\sigma. \tag{3}$$

The transverse force F_y and the aligning moment M_z are then taken to depend only on α, with behaviour generally as illustrated in Figure 2. Finally, there is a damping
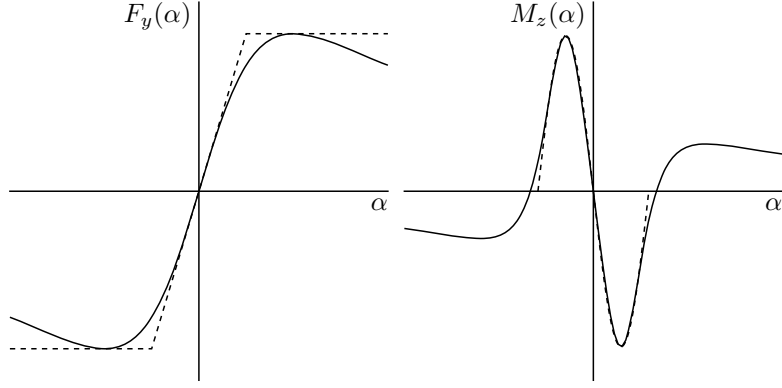
Figure 2: Typical graphs of the side-slip force $F_y(\alpha)$ and self-aligning torque $M_z(\alpha)$.

moment at the tyre which is taken to have the form

$$M_4(\dot\psi/V) = \kappa\dot\psi/V, \qquad (\kappa < 0). \tag{4}$$

2.2 Main equations

The combined system of equations for the model therefore is

$$
\begin{aligned}
I_z\ddot\psi &= M_1(\psi) + M_2(\dot\psi) + M_3(\alpha) + M_4\left(\dot\psi/V\right), & (5)\\
\alpha &= y_1/\sigma, & (6)\\
M_3(\alpha) &= M_z(\alpha) - eF_z(\alpha), & (7)\\
\dot y_1 + \frac{V}{\sigma}y_1 &= V\psi + (e-a)\dot\psi. & (8)
\end{aligned}
$$

The right side of (5) is the net torque about the strut, and the term M_3 given by (7) combines the tyre aligning moment M_z and the moment about the strut of the side force F_y.

2.3 Side force and aligning moment

The nonlinearities in this system are only in the terms $F_y(\alpha)$ and $M_z(\alpha)$ and we discuss briefly the form of these. Each of them is expected to be proportional to the normal force F_z that the tyre is transmitting. During take-off or landing, F_z varies significantly, reducing (to zero) during take-off, and increasing during landing. Nevertheless, for the purposes of this model we treat it as constant, for similar reasons to why we treat V as constant — we are looking for instabilities that occur on a *shorter* timescale than the timescale over which F_z varies significantly. (In reality the tyre contact length a will also vary with F_z, and so for the same reason we treat a as constant here.) Each of F_y and M_z will be an odd function of α, as illustrated in Figure 2. When we scale out by F_z, we denote the slopes of F_y and M_z at the origin by

$$c_{\mathrm{F}} = F_y'(0)/F_z > 0, \qquad c_{\mathrm{M}} = M_z'(0)/F_z < 0. \tag{9}$$

Thus the forms of the functions now become

$$F_y(\alpha) = c_F F_z F_{yn}(\alpha), \qquad M_z(\alpha) = c_M F_z M_{zn}(\alpha), \tag{10}$$

where F_{yn} and M_{zn} are the functions normalized to have $F'_{yn}(0) = 1$ and $M'_{zn}(0) = 1$. Some of the forms used to model measured data on these relationships are

$$F_y(\alpha) = c_1 \operatorname{sgn}(\alpha)\,(1 - \exp(-c_2|\alpha|)) - c_3\alpha, \tag{11}$$

$$F_y(\alpha) = F_{y\,\mathrm{max}} \frac{2\alpha\alpha_{\mathrm{opt}}}{\alpha^2 + \alpha_{\mathrm{opt}}^2}, \tag{12}$$

and these are discussed further in the document [1] that Airbus prepared for the Study Group.

3 Analysis

3.1 Dimensionless model

In a model like this with many parameters, it is important to identify the key dimensionless quantities that govern the behaviour, rather as one identifies the Reynolds number in aerodynamics. By doing this we not only reduce the number of parameters in the system but, more importantly, we focus on the dimensionless ratios that are truly characteristic of the system (rather than physical values that depend on the system of units). A less common use is that if a correctly scaled physical model of the system is to be constructed then it is the dimensionless parameters that have to be matched.

In the present case, it is convenient to rescale physical time t to a dimensionless T given by

$$T = t\sqrt{eF_z/I_z}. \tag{13}$$

We shall take the specific forms of M_1, M_2 and M_4 given by (1) and (4). This then gives the system in the form

$$\psi_{TT} = -\beta_1\psi - \beta_2\psi_T + c_M M_{zn}(\alpha)/e - c_F F_{yn}(\alpha) \tag{14}$$

$$\alpha_T + \epsilon\alpha = \epsilon\psi + \epsilon\beta_3\psi_T. \tag{15}$$

The key nondimensional parameters then are

$$\beta_1 = -\frac{c}{eF_z}, \text{ measuring the torsional spring stiffness of the strut}, \tag{16}$$

$$\beta_2 = -\frac{k + \kappa/V}{(eF_z I_z)^{1/2}}, \text{ measuring the torsional viscous damping}, \tag{17}$$

$$\beta_3 = \frac{e - a}{V}\left(\frac{eF_z}{I_z}\right)^{1/2}, \tag{18}$$

$$\epsilon = \left(\frac{I_z}{eF_z}\right)^{1/2}\frac{V}{\sigma}, \text{ measuring the tyre stiffness}, \tag{19}$$

$$c_F = \text{side-slip force coefficient}, \tag{20}$$

$$c_M = \text{self-aligning torque coefficient}. \tag{21}$$

Note that $\beta_1 > 0$, $\beta_2 > 0$, $\beta_3 > 0$, $\epsilon > 0$, and $c_F > 0$, but $c_M < 0$ (as in [2]). For the representative data in Somieski [2], $e = a$, so we set $\beta_3 = 0$ now. In general though, that term might need to be retained, but it will be small if $e - a$ is small compared to σ. When we take $\beta_3 = 0$, the tyre dynamics equation becomes

$$\alpha_T + \epsilon\alpha = \epsilon\psi. \tag{22}$$

3.2 Linear stability analysis

To carry out the linear stability analysis of the system we let $\phi = \psi_T$ and then the linearized system takes the form

$$\frac{\mathrm{d}}{\mathrm{d}T} \begin{pmatrix} \psi \\ \phi \\ \alpha \end{pmatrix} = \begin{pmatrix} 0 & 1 & 0 \\ -\beta_1 & -\beta_2 & -c_F + \dfrac{c_M}{e} \\ \epsilon & 0 & -\epsilon \end{pmatrix} \begin{pmatrix} \psi \\ \phi \\ \alpha \end{pmatrix}. \tag{23}$$

This matrix has a pair of purely imaginary eigenvalues $\pm i\omega$ when

$$\beta_2\epsilon^2 - \epsilon \left(c_F - \frac{c_M}{e} \right) + \beta_2^2\epsilon + \beta_1\beta_2 = 0, \tag{24}$$

and so this condition on the parameters is the locus on which a Hopf bifurcation occurs. In fact the linearized system is *stable* when

$$\frac{1}{\epsilon} \left(\beta_1 + c_F - \frac{c_M}{e} \right) < \left(1 + \frac{\beta_2}{\epsilon} \right) \left(\beta_2 + \frac{\beta_1}{\epsilon} \right). \tag{25}$$

4 Results

In general, we see from (25) that the linearized system will be stable for β_2 large enough, and unstable when β_2 is small (bearing in mind that $c_F - c_M/e > 0$). So when we plot a stability boundary with β_2 as the vertical axis, the region of stability is *below* some curve. Equally, when we consider variation of ϵ, we see that (25) will hold for ϵ small and for ϵ large, but there may be an intermediate region of instability. So when we plot stability boundaries in the (ϵ, β_2) plane, they will generally be a curve with a single hump, and the system will be stable for parameter values above the curve, and unstable below.

We now present results in which the parameters are taken to have the values in Somieski's paper [2] except that we vary first β_1 and then c_F from their reference values to see how they affect the stability. In fact, for the reference values of β_1, c_F and c_M, the region of (ϵ, β_2) where oscillations occur is the region below the upper curve in Figure 3. However, when β_1 is increased by a factor of 2, or 4, from its reference value then that region of oscillatory behaviour is reduced to the lower curves shown. So these graphs show the stabilizing effect of increasing the torsional stiffness of the landing gear strut.

Next we show the effect of changes in the side-slip force coefficient c_F. We again plot the region of (ϵ, β_2) where oscillations occur, and for the standard parameter values it is the region below the central curve (labelled "Cf") in Figure 4. When the side-slip force coefficient is doubled from its standard value, the region of oscillations is enlarged to the upper curve, and when it is halved the region is reduced.
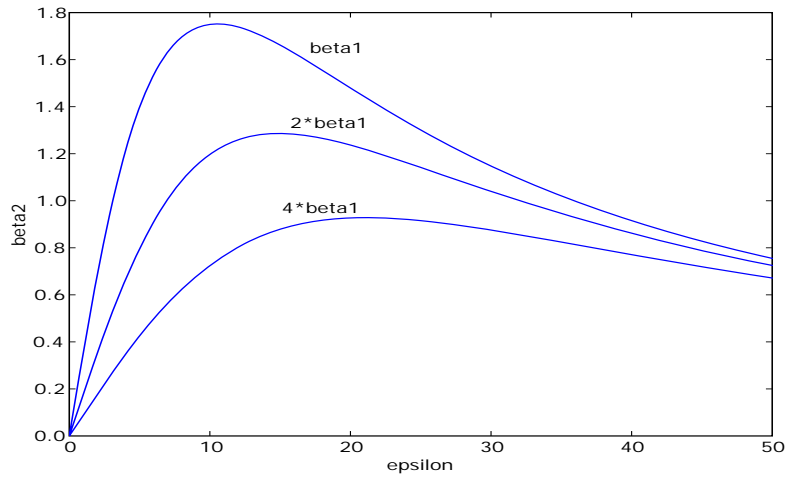
Figure 3: Oscillations occur when (ϵ, β_2) is below the curve. Increasing β_1 (which is proportional to the torsional stiffness of the strut) decreases the region of parameter space where oscillations occur.
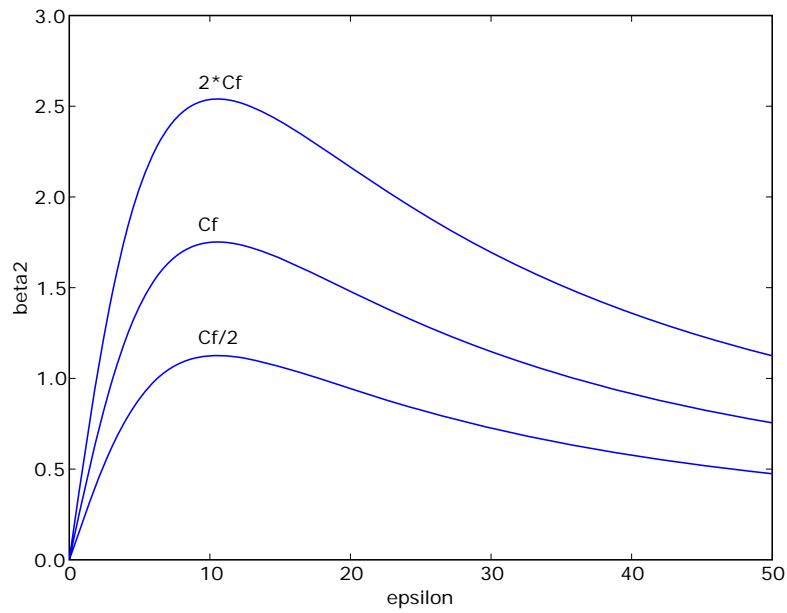
Figure 4: Upper limit of β_2 for stability as a function of ϵ.

4.1 Numerical continuation of nonlinear system

By using the software package AUTO[1] to numerically continue solutions, we find the oscillation amplitude depends on ϵ as illustrated in Figure 5, where the other parameters have been taken to have their reference values. This is effectively running along the
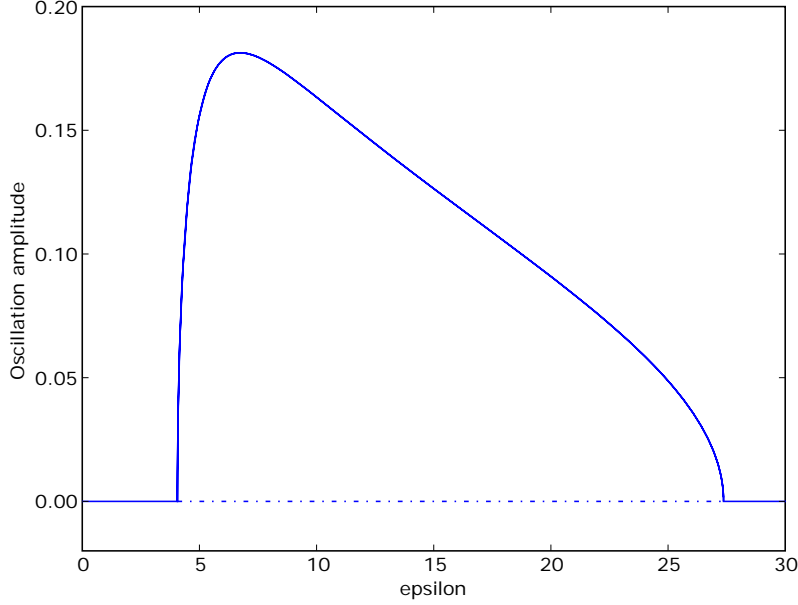
Figure 5: Dependence of oscillation amplitude on ϵ.

horizontal line $\beta_2 \approx 1.4$ in the previous diagrams, and crossing the Hopf bifurcation locus at $\epsilon \approx 4$ and $\epsilon \approx 27$. The fact that the amplitude of the oscillations grows smoothly from zero and returns smoothly to zero suggests that these are each supercritical Hopf bifurcations.

4.2 Hopf bifurcation analysis

Our equations $\psi_{TT} + \beta_2 \psi_T + \beta_1 \psi + F(\alpha) = 0$ and $\alpha_T + \epsilon \alpha = \epsilon \psi$ can be combined into the single equation

$$\frac{1}{\epsilon} \alpha_{TTT} + \left(1 + \frac{\beta_2}{\epsilon}\right) \alpha_{TT} + \left(\beta_2 + \frac{\beta_1}{\epsilon}\right) \alpha_T + \beta_1 \alpha + F(\alpha) = 0, \tag{26}$$

where $F(\alpha) = c_{\mathrm{F}} F_{yn}(\alpha) - c_{\mathrm{M}} M_{zn}(\alpha)/e$ is the only nonlinearity in the system, and is an odd function with $F'(0) = c_{\mathrm{F}} - c_{\mathrm{M}}/e > 0$. For parameter values near equality in (25) we can seek small periodic solutions by the method of harmonic balance, and it is known that if we retain terms at frequencies 0, ω and 2ω and third order in the Taylor series of the nonlinearity, then we obtain an equivalent result to the Hopf bifurcation criterion

---

[1]See http://cmvl.cs.concordia.ca/auto/

for determining whether the bifurcation is supercritical or subcritical. In this case, this approach is particularly simple, since F is an odd function, and so the bifurcated periodic solution will be symmetric about $\alpha = 0$, so we can take

$$\alpha \sim A \cos \omega T + O(A^3)(\cos 3\omega T, \sin 3\omega T) + \dots. \tag{27}$$

Balancing the terms in $\sin \omega T$ in (26) then gives

$$\frac{1}{\epsilon} A \omega^3 - \left(\beta_2 + \frac{\beta_1}{\epsilon}\right) A \omega + O(A^5) = 0, \tag{28}$$

and hence $\omega^2 = \epsilon \beta_2 + \beta_1 + O(A^4)$. Then balancing the terms in $\cos \omega T$ in (26) we get

$$-\left(1 + \frac{\beta_2}{\epsilon}\right) A \omega^2 + (\beta_1 + F'(0)) A + \frac{F'''(0)}{6} A^3 \frac{3}{4} + O(A^5) = 0. \tag{29}$$

So using the value of ω^2 we have

$$\left\{\beta_1 + F'(0) - \left(1 + \frac{\beta_2}{\epsilon}\right)(\epsilon \beta_2 + \beta_1)\right\} + \frac{F'''(0)A^2}{8} = O(A^4). \tag{30}$$

Here the quantity in braces $\{.\}$ is positive when the equilibrium is unstable, so the bifurcation is supercritical if and only if $F'''(0) < 0$. This applies to the bifurcations at both the upper and lower ends of the range of ϵ values. If F_y and M_z are represented by functions of the form (12) then this will certainly be the case, and the bifurcations will be supercritical. The fit by (11) does not have a third derivative at $\alpha = 0$ but any regularization of the singularity there will give $F'''(0) < 0$ (since $F''(0-) > 0 > F''(0+)$) so again we would expect the use of that form to give supercritical bifurcations.

However, it is observed in practice that there is hysteresis with shimmy: when the aircraft velocity is increased, shimmy begins at some velocity V_1, and when the velocity is then decreased, shimmy persists until V falls below some $V_2 < V_1$. This shows that the real bifurcation diagram is certainly more complex than illustrated in Figure 5 and possibly that there is a subcritical Hopf bifurcation.

5 Extensions

Some of the further work that could be considered includes

- Two-tyre model. When a 2-tyre landing gear is considered, it is expected that longitudinal forces will play a role. Gyroscopic effects may also be relevant, since they will alter the way the vertical load is shared between the tyres. If the tyres are identical there may be a reduction to the 1-tyre model, but slight asymmetry of the tyres will complicate the situation.

- A further improvement to the model would be to model the tyre dynamics more realistically, and in particular to include tyre 'memory' effects, *i.e.* the fact that the different regions of the tyre's contact with the ground were 'laid down' at different stages of its rolling contact, so there are really delay terms in F_y and M_z instead of the simple functional dependence on the instantaneous value of α that has been taken here.

6 Conclusions

We have shown that a simple lumped parameter third-order model does exhibit shimmy, and can give the observed effect of shimmy occurring for a certain interval of forward velocities. The linear stability analysis gives 'safe' regions of parameter space, in which the system is linearly stable, and these depend on the system parameters in the expected way, *e.g.* increasing the torsional stiffness of the strut reduces the region of parameter space where oscillations occur. Numerical simulation of the nonlinear system with AUTO produces oscillations that grow smoothly (but rapidly) from equilibrium as the parameter ϵ is increased through the lower critical value, and decrease smoothly to zero as ϵ passes through the upper critical value.

7 Notation

a half-length of tyre contact with ground, equation (2)
A amplitude of shimmy oscillation in Hopf bifurcation analysis, (27)
c torsional stiffness of strut, (1)
$c_{1,2,3}$ constants in fitted side-force curve, (11)
c_{F} side-slip force coefficient: slope of tyre side force curve at $\alpha = 0$, (9)
c_{M} self-aligning torque coefficient: slope of tyre aligning moment curve at $\alpha = 0$, (9)
e caster length, Figure 1
$F(\alpha)$ combined nonlinearity due to tyre contact force and moment, (26)
F_y side force at tyre contact, Figure 1
$F_{y\,\mathrm{max}}$ maximum side force, (12)
F_{yn} normalized side force, (10)
I_z moment of inertia of landing gear about strut, (5)
k torsional damping constant of strut, (1)
M_1 torsional moment in landing gear strut, Figure 1
M_2 damping moment in landing gear strut, Figure 1
M_3 net moment of tyre forces about strut (7)
M_4 damping moment at tyre contact, Figure 1
M_z aligning moment at tyre contact, Figure 1
M_{zn} normalized aligning moment, (10)
t time
T dimensionless rescaled time, (13)
V forward velocity of aircraft, Figure 1
x horizontal coordinate along the direction of motion, Figure 1
y horizontal coordinate perpendicular to the direction of motion, Figure 1
y_1 transverse deviation of tyre leading contact point, (2)
α slip angle, (3)
α_{opt} slip angle giving maximum side force, (12)
β_1 dimensionless parameter measuring torsional stiffness of the strut, (16)
β_2 dimensionless parameter measuring torsional damping in the strut, (17)
β_3 dimensionless parameter in tyre dynamics equation, (18)

ϵ	dimensionless parameter measuring tyre stiffness, (19)
κ	torsional damping constant of tyre contact, (4)
σ	relaxation length for transverse deflection of tyre, (2)
ψ	yaw angle of landing gear, Figure 1
ω	radian frequency of shimmy oscillation in Hopf bifurcation analysis, (27)

References

[1] Landing Gear Shimmy. Airbus document provided to the Study Group by Etienne Coetzee.

[2] Shimmy analysis of a simple aircraft nose landing gear model using different mathematical methods. Gerhard Somieski, Aerospace Science and Technology **8**, 545–555, 1997.

[3] Appell-Gibbs equations for classical wheel shimmy—an energy view. Gábor Stépán, Journal of Computational and Applied Mechanics **3**, 85–92, 2002.

[4] Delay, nonlinear oscillations and shimmying wheels. G. Stépán. pp 373–386 of *Applications of nonlinear and chaotic dynamics in mechanics*, Kluwer Academic Publisher (Dordrecht), ed. F.C. Moon, 1998.